CHAPTER 9
PRELIMINARY SHUTTLE SPACE SUIT SHIELDING MODEL

Brooke M. Anderson
George Washington University
Hampton, Virginia

J. E. Nealy
Old Dominion University
Norfolk, Virginia

G.D. Qualls, P.J. Staritz, J.W. Wilson
NASA Langley Research Center
Hampton, Virginia

M.-H. Y. Kim
College of William and Mary
Williamsburg, Virginia

F. A. Cucinotta
NASA Johnson Space Center
Houston, Texas

W. Atwell
The Boeing Co.
Houston, Texas

G. De Angelis
NASA Langley Research Center
Hampton, Virginia
& Istituto Superiore di Sanita'
Rome, Italy

J. Ware, A. E. Persans
ILC Dover
Frederica, Delaware

PRELIMINARY SHUTTLE SPACE SUIT SHIELDING MODEL

9.1 INTRODUCTION

A detailed space suit computational model is being developed at the Langley Research Center for exposure evaluation studies. The details of the construction of the space suit are critical to an estimate of exposures and for assessing the risk to the astronaut during EVA. Fine detail of the basic fabric structure, helmet, and backpack is required to assure a valid evaluation. The exposure fields within the computerized anatomical male (CAM) and female (CAF) are evaluated at 155 and 160 points, respectively, to determine the dose fluctuations within critical organs. Exposure evaluations for ambient environments will be given and potential implications for geomagnetic storm conditions discussed.

It has been stated that ISS will require up to 1500 hours of EVA during its construction and 400 hours of EVA per year in operations and maintenance. The 51.6° inclination of the ISS orbit provides a highly variable radiation environment driven by solar activity. SPEs will adversely impact the radiation environment in this region, especially in the case of an associated geomagnetic storm, during which the region of influence is expanded during the storm main phase [1]. The geomagnetic storm conditions also increase the strength of the trapped electron environment by up to four orders of magnitude; this electron enhancement can persist for several days. Even under quiet field conditions, the distribution of dose within the body is vastly different than that experienced within ISS and dose gradients near the body surface are important to the evaluation of effective dose as related to cancer and cataract risks. This gradient is related to the material make-up of the space suit about critical body organs and enhancements of the electron environment during times of geomagnetic activity.

There are two space suits in current usage within the space program: EMU [2] and Orlan-M Space Suit [3,4]. The Shuttle space suit components are discussed elsewhere [2,5,6] and serve as a guide to development of the current model. The present model is somewhat simplified in details which are considered to be second order in their effects on exposures. A more systematic approach is ongoing on a part-by-part basis with the most important ones in terms of exposure contributions being addressed first with detailed studies of the relatively thin space suit fabric as the first example [7]. Additional studies to validate the model of the head coverings (bubble, helmet, visors…) will be undertaken in the near future. The purpose of this paper is to present the details of the model as it is now and to examine its impact on estimates of astronaut health risks. In this respect, the nonuniform distribution of mass of the space suit provides increased shielding in some directions and some organs. These effects can be most important in terms of health risks [8] and especially critical to evaluation of potential early radiation effects [9].

9.2 SPACE SUIT DESCRIPTION

The basic space suit assembly is shown in **Figure 9-1**. The LCVG fits close to the body and is constructed of Spandex, Nylon net, and ethylvinylacetate tubing filled with circulating water. The areal density of the Spandex/Nylon net is 0.076 g/cm^2 and the 4-mm o.d. tube is 0.078 g/cm (including water); they are inserted in the Spandex at the rate of 1 tube per centimeter (**Figure 9-2**). The usual approximation of the LCVG material is

0.154 g/cm^2 as used by Kosmo et al. [5]. The inadequacy of this approximation is thoroughly discussed in [7]. The communications carrier assembly is currently not represented in the model. The helmet with its internal vent deflector is constructed of polycarbonate, as is the protective visor of the EVVA. The remaining visors are constructed of polysulfone. The assembly has an inner Teflon liner and is covered by an Orthofabric for mechanical protection, aluminized Mylar for thermal insulation, and Dacron. The material list is given in **Table 9-1**.

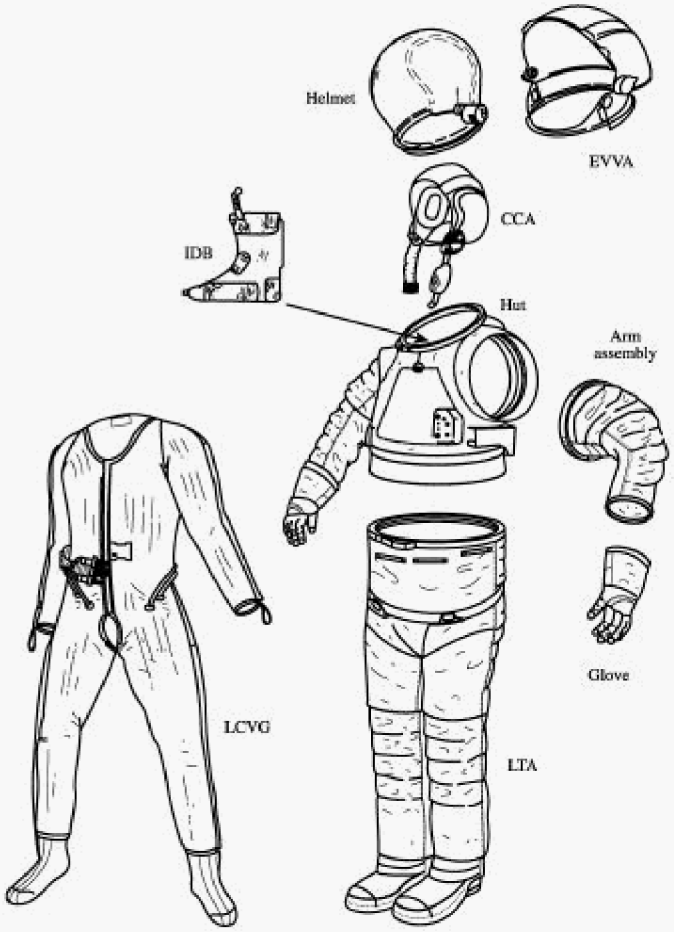

Figure 9-1. Basic components of the Shuttle space suit.

Table 9-1. Material Layups of Helmet and Extravehicular Visor Assembly

Layer	Material	Areal Density, g/cm^2
Outer layer	Orthofabric-Teflon/Nomex/Kevlar	0.049
Insulation	Aluminized Mylar- 5 plys	0.014
Spacer	Dacron fiber- 5 plys	0.011
Inner liner	Teflon	0.028
Extravehicular visor assembly shell	Polycarbonate	0.381
Sun visor	Polysulfone	0.190
Eye shade	Polysulfone	0.190
Protective visor	Polycarbonate	0.182
Helmet	Polycarbonate	0.182

The remainder of the suit consists of the HUT, the arm assemblies including gloves, and the LTA. The HUT main body is constructed of Fiberglas and covered outside with Orthofabric, aluminized Mylar, and Neoprene-coated Nylon ripstop. Under the HUT is the LCVG next to the astronaut body. The material layup in the HUT region of the suit is given in **Table 9-2**. The arm assemblies and LTA are made of fabric and water-filled cooling tubes. The fabric layups are shown in **Figure 9-2** and described in **Table 9-3** and [6]. The fabrics of the arm assembly and LTA, gloves, and boots are given a simplified representation in the present model. For example, there is additional fabric in locations where bending occurs to allow flexibility. These will be modeled later in the next level of detail.

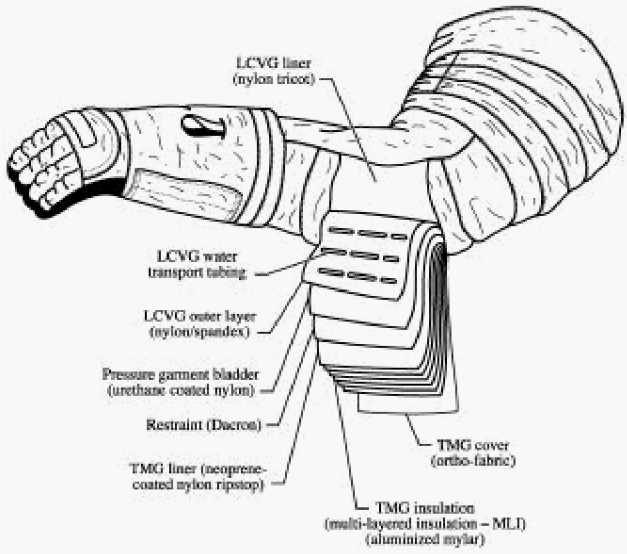

Figure 9-2. Cross section of material layup.

Table 9-2. Material Layups of the Hard Upper Torso

Layer	Material	Areal density, g/cm^2
Outer layer	Orthofabric-Teflon/Nomex/Kevlar	0.049
Insulation	Aluminized Mylar- 5 plys	0.014
Inner liner	Neoprene coated Nylon ripstop	0.028
Hard shell	Fiberglas	0.354
LCVG	Spandex/water/ethylvinylacetate	0.154

Table 9-3. Material Layup of the Space Suit Fabric and Water-Filled Tube [2,7]

Material	Areal density, g/cm^2
Orthofabric-Teflon/Nomex/Kevlar	0.049
Reinforced aluminized Mylar	0.014
Neoprene coated ripstop	0.028
Dacron® Polyester	0.021
Urethane Coated Nylon	0.014
Nylon/Spandex/water/ethylvinylacetate	0.154

An important component of the space suit shield model is the portable life support system (PLSS) shown in **Figure 9-3**. Not shown in the figure are the secondary oxygen tanks that attach to the lower section of the PLSS. Approximate estimates of material mass of various subsystems and overall dimensions are given in **Table 9-4**. As seen in the table, a major fraction of the mass of the extravehicular maneuvering unit (EMU) is associated with the backpack and is expected to be important in providing protection to internal organs.

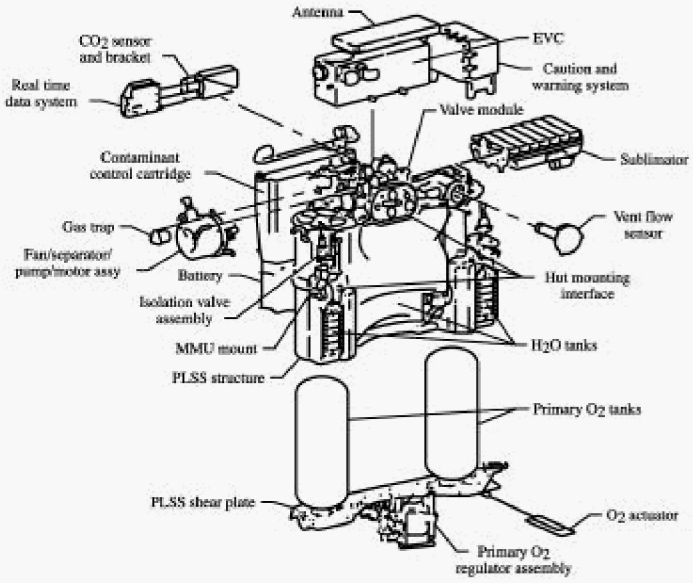

Figure 9-3. EMU portable life support system.

The geometric arrangement of materials in **Tables 9-1** to **9-4** will then provide a preliminary model of the space suit. Although the description is somewhat simplified, this is the most complete shielding model to date. This is an important step in understanding the expected exposures in ISS operations and will be useful in mission planning.

9.3 SPACE SUIT MODEL

The preliminary space suit model is implemented using the CAD geometry package of IDEAS[2] software. The geometry is simplified but represents the location of major massive components and the distribution of fabric and other components about an astronaut within the suit cavity. The CAD derived model is shown in **Figure 9-4**.

Table 9-4. Approximate Material and Dimensions of Portable Life Support System

Subsystem	Materials	Mass, kg	Dimensions, inch (h,w,d)
O_2 Ventilating Circuit:			
Regulators, vessels, fans…	Fe, Cr, Ni, Cu…	14.4	
LiOH assembly	LiOH, Fe	6.4	
H_2O transport:			
Pump, valves, sensors	Fe, Cu	6.5	
Liquid	H_2O	4.5	
Electrical system:			
Electronics	Si, O, Cu…	15.1	
Battery	ZnAgO	4.5	
O_2 purge system:			
Bottles	Fe, O	8.6	
Regulator	Fe	4.2	
Total		65.2	$25 \times 23 \times 7$

In the model, it is assumed that the Spandex/Nylon net of the LCVG are part of the suit fabric and that the ethylvinylacetate tubes filled with water are lying on the skin surface except for the head, hands, and feet. In testing, it is found that the fabric of **Table 9-3** (less the water-filled tube) presents a distribution [7] of material along a given path that is random according to

$$p(t) = exp[-(t-t_o)^2/(2\sigma^2)]/(2\pi\sigma^2)^{1/2} \qquad (1)$$

where the mean thickness t_o is 0.161 g/cm^2 and σ is 0.03 g/cm^2. It is assumed that each ray through the fabric is scaled according the distribution (1). In the CAD model the fabric is of fixed thickness t_{min} but rays passing through the surface in direction $\boldsymbol{\Omega}$ see thickness along the slant height $t_m(\boldsymbol{\Omega})$ and needs relation to the fabric distribution (1). The ray thickness is then taken as a random variable in which

$$t_{ray}(\boldsymbol{\Omega}) = t(\kappa)t_m(\boldsymbol{\Omega}) /t_{min} \qquad (2)$$

where κ is a uniform random number on the interval {0,1} and

$$t(\kappa) = t_o + 2^{1/2}\ \sigma erf^{-1}(2\ \kappa - 1) \qquad (3)$$

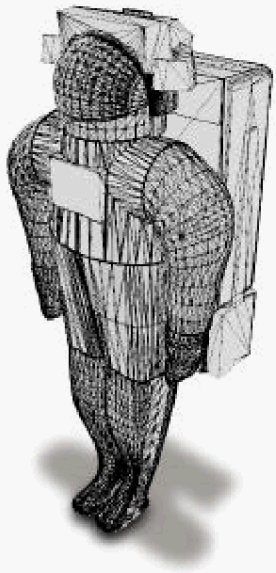

Figure 9-4. CAD model in faceted representation.

where erf^{-1} is the inverse error function and a different random number κ is taken for each ray direction. The scaling in equation (2) represents the nonuniformity in the fabric observed in transmission testing [7].

The water-filled tubes are likewise complicated in their representation within the CAD model. The tubes are located in parallel arrays separated by 1 cm [7]. Since the tubes are held on the skin of the astronaut (represented by the CAM or CAF models) and an arbitrary point in the astronaut's body at which the exposure is to be evaluated can be considered randomly, then the problem is to find the probability that the rays passing through the dose point in fact passed through a section of a water-filled tube. The tubes are mainly important to the skin points located near a tube. Points remote from any tube (e.g., deep in the body) are little affected. Since the tubes are parallel and 1 cm apart, then each point will only consider the two nearest tubes. This is accomplished as follows.

The nearest tube to the dose point will lie near the ray of minimum distance to the surface of the skin. This ray direction $\boldsymbol{\Omega}_{min}$ is found by searching over the body thickness function $t_b(\boldsymbol{\Omega})$ for the smallest value. At that point on the surface with minimum thickness to the dose point, we place two tubes on opposite sides, one located at a distance $x(\kappa)$ given as

$$x(\kappa) = 0.5\ \kappa\ (cm) \qquad (4)$$

where the second tube is at a distance $1 - x(\kappa)$ and κ is a uniformly distributed random number on the interval {0,1} as before. However, whereas each direction $\boldsymbol{\Omega}$ has a separate κ in equation (2), there is only one κ for each dose point in equation (4). For a given $x(\kappa)$ and direction $\boldsymbol{\Omega}$, we require the chord through either of the two tubes. To calculate this chord, we require solving the appropriate geometry. The first step is to define a coordinate system. Since $\boldsymbol{\Omega}_{min}$ is assumed normal to the local surface, then any unit vector $\boldsymbol{\beta}$ such that $\boldsymbol{\beta}\cdot\boldsymbol{\Omega}_{min} = 0$ is tangent to the local

surface. We will use an arbitrary tangent vector to define the direction to the tube and a unit vector $\boldsymbol{\gamma}$ parallel to the tube axis for the calculations. We take

$$\boldsymbol{\beta}\cdot\boldsymbol{\Omega}_{min} = \beta_1\alpha_1 + \beta_2\alpha_2 + \beta_3\alpha_3 = 0 \tag{5}$$

which we solve by finding $\alpha_{Im} = min\{\alpha_I\}$ and set $\beta_{im} = 0$. The remaining β_I can be solved with the requirement of normalization to unity. The vector parallel to the tube is given as

$$\boldsymbol{\gamma} = \boldsymbol{\beta} \times \boldsymbol{\Omega}_{min} \tag{6}$$

The point on the tube axis located at $x(\kappa)$ along the surface nearest the dose point as defined above is

$$\boldsymbol{x}_{tube} = t(\boldsymbol{\Omega}_{min})\,\boldsymbol{\Omega}_{min} + x(\kappa)\boldsymbol{\beta} \tag{7}$$

An arbitrary point on the tube axis is given as

$$\boldsymbol{x}(s) = \boldsymbol{x}_{tube} + s\,\boldsymbol{\gamma} \tag{8}$$

where s is the distance along the tube measured from the point on the tube nearest the dose point. We need the nearest point to the tube axis along an arbitrary direction $\boldsymbol{\Omega}$ to evaluate the chord for that ray. This is accomplished by finding the minimum of the distance D as

$$D^2 = Min_{\,s,v}\,\{\,[\boldsymbol{x}(s) - v\,\boldsymbol{\Omega}]^2\} \tag{9}$$

The solution can be written as

$$D^2 = [t(\boldsymbol{\Omega}_{min}) - v\,\omega_1]^2 + [x(\kappa) - v\,\omega_2]^2 \tag{10}$$

where

$$v = [t(\boldsymbol{\Omega}_{min})\,\omega_1 + x(\kappa)\,\omega_2]/[\,\omega_1^2 + \omega_2^2] \tag{11}$$

The chord is, for D less than the tube radius r_0, given as

$$C = 2\,[r_o^2 - D^2]^{1/2} \tag{12}$$

and has value zero for values of D greater than r_o. The material the ray must penetrate to reach the astronaut within the suit is the chord so that the total shielding is

$$t_{ray}(\boldsymbol{\Omega}) = t(\kappa)t_m(\boldsymbol{\Omega})\,/t_{min} + C \tag{13}$$

Note, even if an intersection of the tube at $x(\kappa)$ is not found the calculation is to be repeated by replacing $x(\kappa)$ with $x(\kappa) - 1$ for the second tube of the nearest pair. The chord of the next nearest pair is evaluated by replacing the $x(\kappa)$ by $x(\kappa) + 1$ and then by $x(\kappa)$ -2. The appropriate value(s) of C is (are) used (summed) in equation (13).

The CAD model of the space suit is used to generate shielding distributions about the dose points chosen in the CAM and CAF models and will be modified according to the above analysis to represent the materials about the dose points.

9.4 HUMAN GEOMETRY MODEL

The CAM model was first developed by Kase [10] in 1970. Numerous errors were discovered in the combinatorial geometry, and Billings and Yucker [11] corrected the geometrical representation in 1973 using a QUAD geometry modeling technique [12] where geometrical regions and surfaces are used to represent the 50th percentile U.S. Air Force male. The model is very detailed, comprising some 1100 unique geometric surfaces and approximately 2400 solid regions. The internal body geometry, such as critical body organs, voids, bone, and bone marrow, are explicitly modeled with the proper chemical composition and density. A supporting program called CAMERA was developed to perform analyses on the model, which include ray tracing to generate shielding distributions for any point in and on the CAM model. CAMERA also has the capability to generate cross-sectional views of the coordinate (dose) point of interest.

With the increase of females being assigned to fly on Shuttle missions, Yucker and Huston [13] developed the CAF model. Using the existing CAM model, they "removed" the male organs and "replaced" them with the appropriate female organs (breast, uterus, and ovaries). Since the average female is approximately 92% the size of the average male, the CAF was scaled accordingly.

Since astronauts come in all sizes, Yucker [15] developed a three-dimensional scaling capability, and Atwell [16,17] later refined and made several corrections to the CAF model. The CAM and CAF models have been used extensively to compute astronaut body organ exposures for the Space Shuttle and ISS programs.

9.5 ENVIRONMENTAL MODELS

The environments of concern are the LEO environment of ISS and the deep space (beyond the geomagnetic field) environment. They differ on account of the geomagnetic field. Although the GCRs are part of the over all exposure, only the trapped radiations during quiet geomagnetic periods will be considered in LEO and the SPEs in deep space.

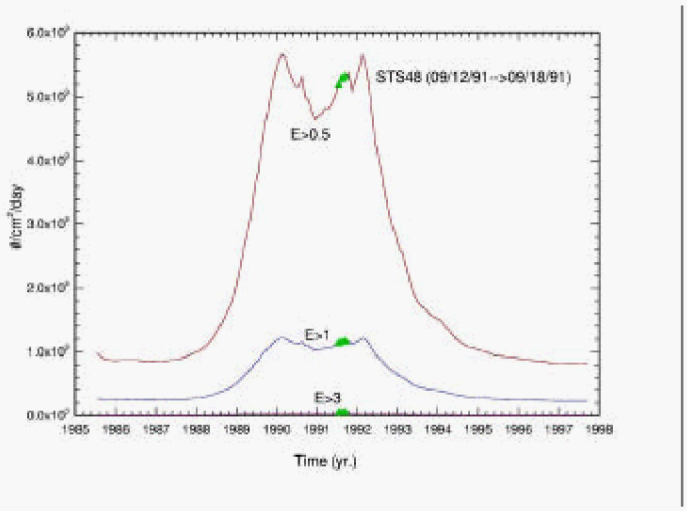

Figure 9-5. STS-48 electron environment.

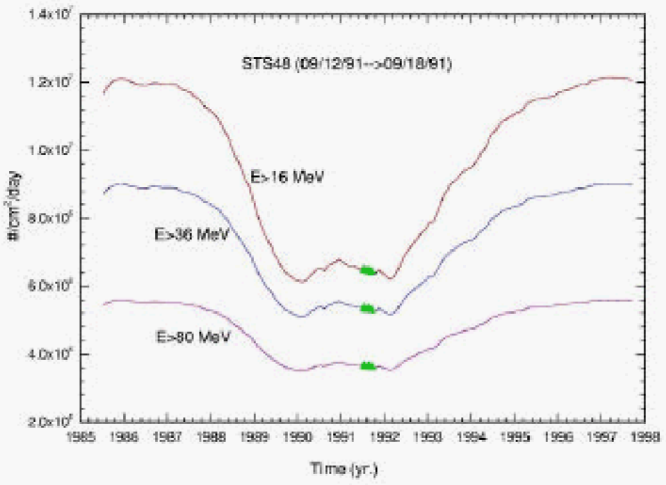

Figure 9-6. STS-48 proton environment.

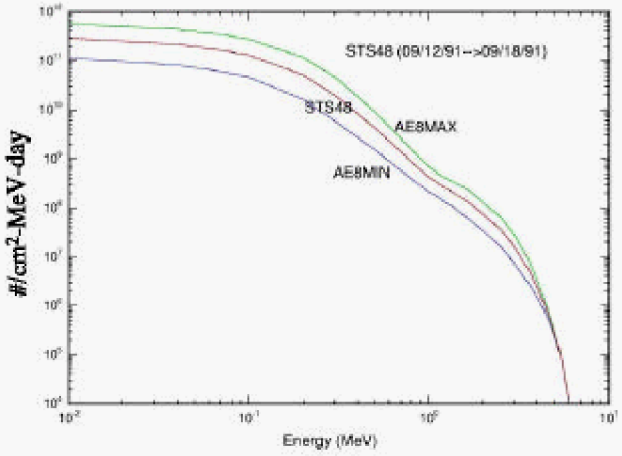

Figure 9-7. STS-48 electron environment compared to AE8 model.

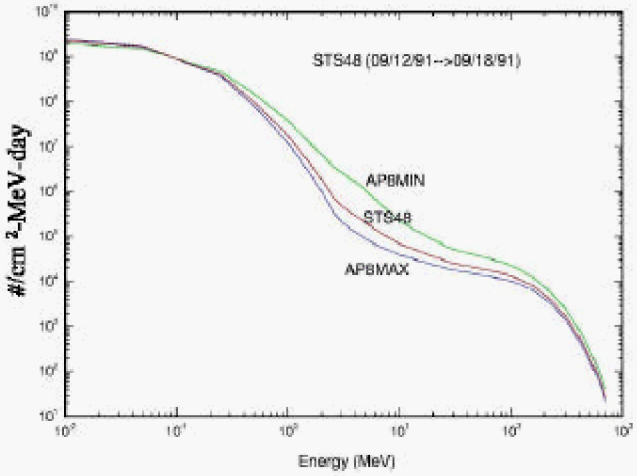

Figure 9-8. STS-48 proton environment compared to AP8 model.

Even during geomagnetic quiet times, the particle fields are variable over the solar cycle. The time-dependent fields are shown relative to the Sept. 1991 flight environment of STS-48 at 313 nmi and 57° in **Figures 9-5** and **9-6** as evaluated by a recently derived model [17]. The model utilizes the environmental maps of AE8 and AP8 with superimposed solar cycle variations related to particle source and loss terms. The STS-48 spectra during Sept. 1991 are compared to the base models at solar maximum and minimum in **Figures 9-7** and **9-8**. The GCR background will be ignored in the present calculation. The solar energetic particles are deflected in the geomagnetic field and will be ignored in the present study, although they can be an important contribution especially during geomagnetic storms [1]. Even more common and troubling are large geomagnetic disturbances and the associated increase in the trapped electron environment by three or four orders of magnitude lasting for several days.

SPEs in deep space operations are of great concern, since a lethal exposure can be received over a several-hour period [18] and the resultant biological response will be serious. This is especially true in a space suit, where only minimal protection is available [18]. The largest observed high-energy event is that of Feb. 23, 1956, with the second-largest such event being an order-of-magnitude smaller, occurring on Sept. 29, 1989. The Feb. 23, 1956, event was only observed on the ground, and the spectrum at low energies is most uncertain. It has been suggested that the Sept. 29, 1989, event where detailed measurements exists should be scaled by perhaps a factor of 10 and used as the event appropriate for design. Studies have shown that such an event would provide a considerable health risk to the astronaut although an overly simplified space suit model was used [19]. The fluence spectra of the Sept. 29, 1989, event [19] are shown in **Figures 9-9** and **9-10**.

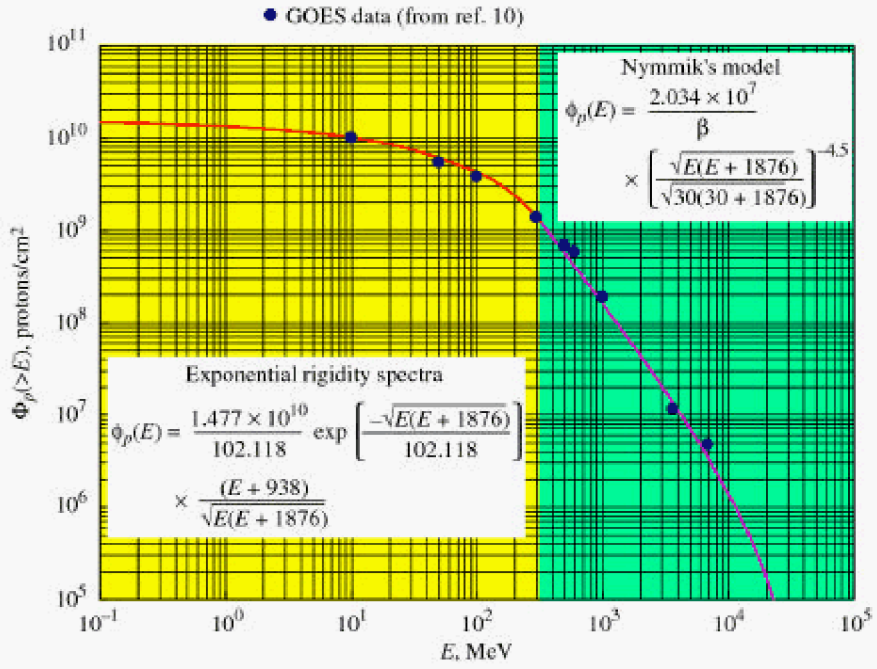

Figure 9-9. Sept. 29, 1989, solar proton spectrum.

The low-level GCR exposures appear as background and will be ignored in the present study. The present emphasis is on the short-term exposures, although the background from the trapped particles in LEO during

geomagnetic quiet times is evaluated to estimate the dose during large electron population variations under disturbed geomagnetic conditions.

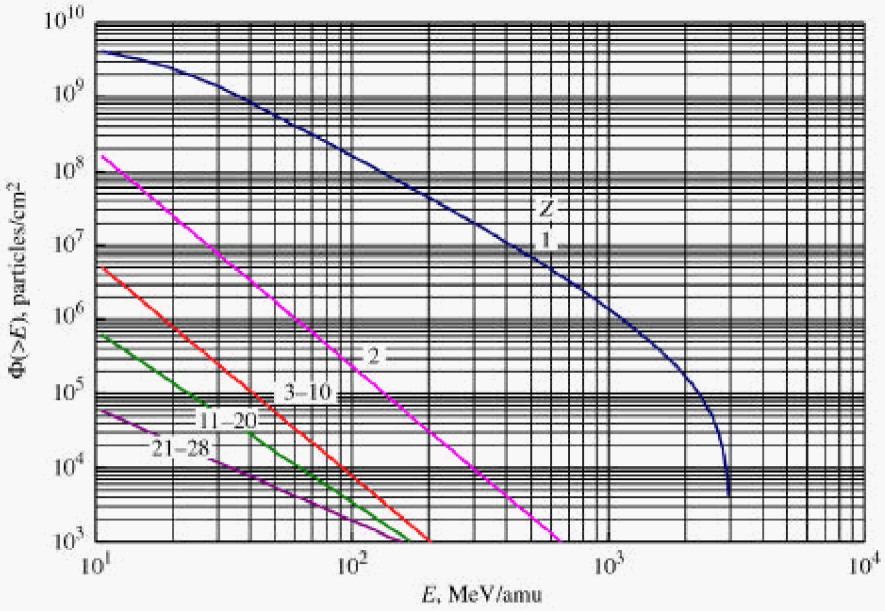

Figure 9-10. Sept. 29, 1989, solar heavy ion spectra.

9.6 COMPUTATIONAL PROCEDURES

The types and energy distributions of particles transmitted through a shield material require the solution to the Boltzmann transport equation with appropriate boundary conditions related to the external space radiation environment. The relevant transport equation [20] for the flux density $\phi_j(\boldsymbol{x},\boldsymbol{\Omega},E)$ of type j particles moving in direction $\boldsymbol{\Omega}$ with energy E is given as

$$\boldsymbol{\Omega}\bullet\boldsymbol{\nabla}\phi_j(\boldsymbol{x},\boldsymbol{\Omega},E) = ? \int \sigma_{jk}(\boldsymbol{\Omega},\boldsymbol{\Omega}',E,E')\ \phi_k(\boldsymbol{x},\boldsymbol{\Omega}',E')\ d\boldsymbol{\Omega}'\ dE' - \sigma_j(E)\ \phi_j(\boldsymbol{x},\boldsymbol{\Omega},E) \qquad (14)$$

where $\sigma_j(E)$ is the media macroscopic cross section for removal of j particles of energy E, $\sigma_{jk}(\boldsymbol{\Omega},\boldsymbol{\Omega}',E,E')$ are the media macroscopic cross sections for various atomic and nuclear processes adding j particles of energy E in direction $\boldsymbol{\Omega}$ including spontaneous disintegration. In general, there are hundreds of particle fields $\phi_j(\boldsymbol{x},\boldsymbol{\Omega},E)$ with several thousand cross-coupling terms $\sigma_{jk}(\boldsymbol{\Omega},\boldsymbol{\Omega}',E,E')$ through the integral in equation (14). The total cross section $\sigma_j(E)$ with the medium for each particle type of energy E may be expanded as

$$\sigma_j\ (E) = \sigma_{j,at}\ (E) + \sigma_{j,el}\ (E) + \sigma_{j,r}\ (E) \qquad (15)$$

where the first term refers to collision with atomic electrons, the second term is for elastic nuclear scattering, and the third term describes nuclear reactive processes and is ordered as $1{:}10^{-5}{:}10^{-8}$. This ordering allows flexibility in expanding solutions to the Boltzmann equation as a sequence of physical perturbative approximations. The atomic interactions are treated using energy moments in which the leading term is the usual continuous slowing down approximation. Special problems arise in the perturbation approach for neutrons for which the nuclear elastic process appears as the first-order perturbation and has been the recent focus of research [21].

The electrons have negligible nuclear reaction cross sections and are dominated by atomic and elastic processes. The basic electron transport is treated by invoking the "continuous-slowing-down-approximation" range, where the usual "continuous-slowing-down-approximation" range has been modified parametrically to account for shortened path length due to multiple scattering. The practical ranges and corresponding range-energy relations are derived from the parameterizations of Tabata et al. [22]. For an electron of initial energy, E, its residual energy, W, after going distance, t, in an attenuating medium may be found by solving the equation

$$R(W) = R(E) - t \tag{16}$$

for W when the practical range $R(W) > 0$. Effects of energy fluctuations are incorporated using the energy dissipation formulation of Kobetich and Katz [23,24], in which actual energy dissipation, G, is expressed in terms of a transmission function, η, as

$$G = d(\eta W)/dt \tag{17}$$

The parameterizations for R and η have been based on numerous electron beam experiments for energy ranges and material elements applicable to space radiation calculations.

The dose at distance t for electron differential flux ϕ_e may then be expressed in terms of the initial and final energy spectra [25]

$$D(t) = \int G(E,t)\ \phi_e(E)dE = \int S(W)\ \phi_e(W)dW \tag{18}$$

where S is stopping power. In conformance with the "continuous-slowing-down-approximation" range, the emerging electron spectrum may then be expressed in terms of the initial spectrum as [25]

$$\phi_e(W) = \phi_e(E)G(E)S(E)/[S(W)]^2 \tag{19}$$

In passing through condensed matter, the decelerating electrons give rise to energetic photons (bremsstrahlung), which also contribute to the total energy deposition. The photon production may be expressed in terms of a differential cross section, $\sigma(W,E')$, which represents a probability that an electron of energy W produces a photon of energy E' in its interaction with an atom of the material. These cross sections are generally complicated functions of W, E', and material composition. They have been extensively tabulated by Seltzer and Berger [26] for wide energy ranges and most elements of the periodic chart. The effective production cross sections for a given material are determined in the present calculations by appropriate spline interpolations of the Berger-Seltzer tabulations.

The photon source term, ς, at distance x and energy E' may be calculated from the electron spectrum as

$$\varsigma(x, E') = \int_{E'}^{W(x)} \phi_e\ \sigma(W, E')\ dW \tag{20}$$

The photons are also being attenuated in accordance with an extinction coefficient, μ, and the photon differential spectrum, $\phi_p(E')$, at distance t may be found using the transfer equation

$$\phi_p(E') = \int \varsigma(x, E')\ e^{-\mu(t-x)}\ dx \tag{21}$$

and the subsequent energy deposition as

$$D_p(t) = \int \mu_e E'\ \phi_p(E')d\,E' \tag{22}$$

where μ_e is an absorption coefficient for photon energy loss resulting in ionizing energy deposition (generally less than the total extinction coefficient, μ). The present code formulation assumes all photons generated propagate in the direction of electron motion.

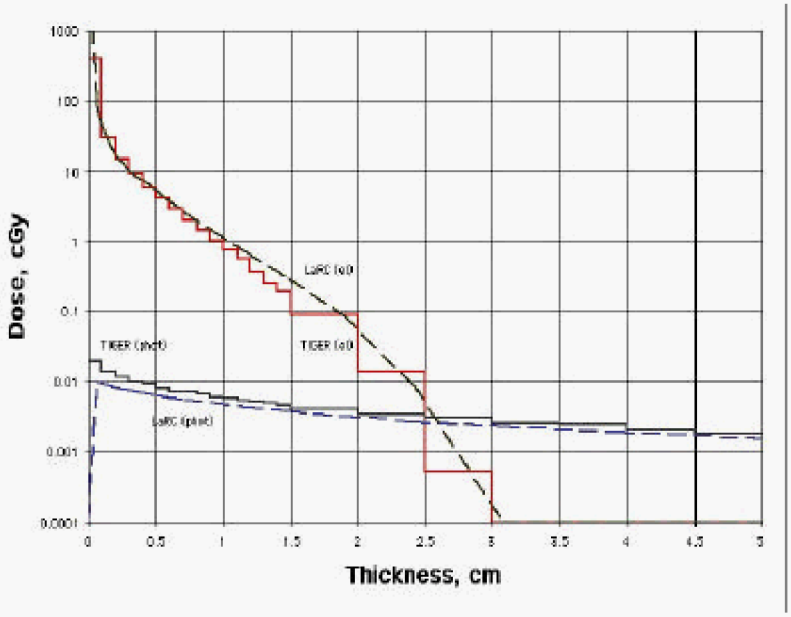

Figure 9-11. STS-63 electron generated dose in a water shield of the present model and TIGERP.

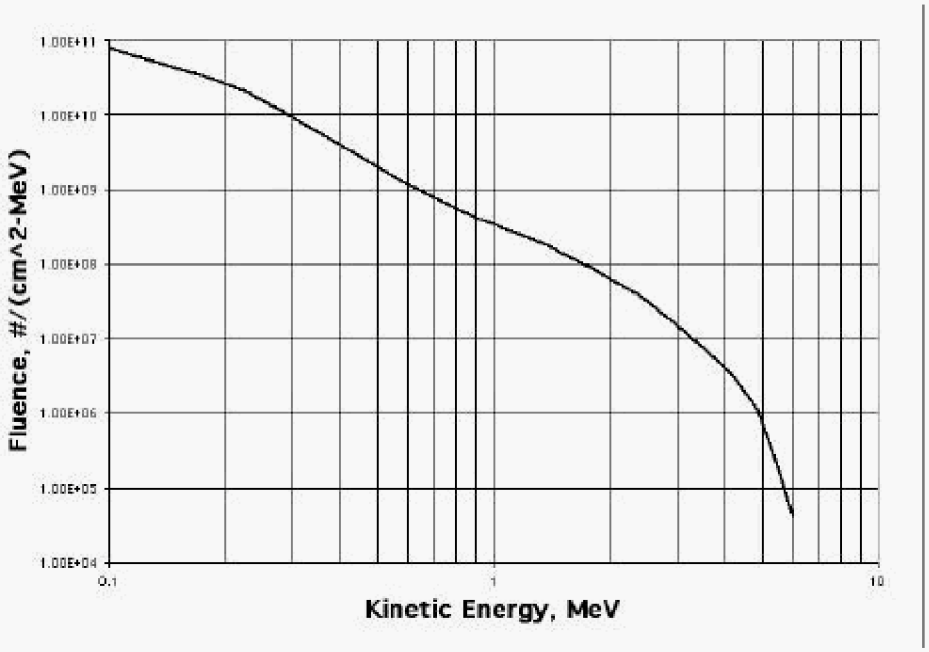

Figure 9-12. Ten-day electron fluence for STS-63.

This simple procedure is of recent vintage, and validation and benchmarking continue at the present time. Calculations for benchmark comparisons made thus far indicate that accuracy has not been substantially degraded at the expense of computational speed. An example of a comparison calculation is given in **Figure 9-11** for the electron fluence spectrum shown in **Figure 9-12** appropriate to the STS-63 10-day mission at 213 nmi (392 km) at

51.6° inclination and is propagated at normal incidence through a semi-infinite water slab. The Monte Carlo code TIGERP [27] was used to validate the computation and the very favorable comparison is evident.

9.7 RESULTS

The dose at a location within the astronaut's body depends on the surrounding space suit materials and body tissues. The space suit material's distributions are evaluated along 1922 ray directions associated with a fixed solid angle ($\Delta\Omega = 4\pi/1922$) as discussed elsewhere [29]. Various three-dimensional visualization techniques are useful in understanding these distributions. For example, the projected rays through the space suit materials about a location in the sternum are shown in **Figure 9-13**. The potential role of the EMU lights and camera, the backpack, and the display control module are clearly evident.

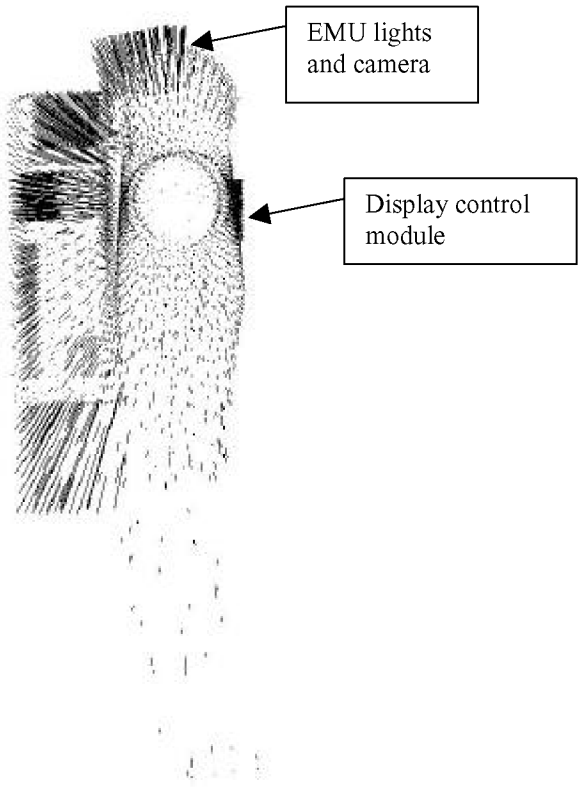

Figure 9-13. Projected space suit material crossings along 1922 ray directions.

Another visualization device is shown in **Figure 9-14** where the gray scale (normally color is used) displays the relative shielding about the dose point. For online analysis, the spherical shape in **Figure 9-14** is rotated to fully examine the total solid angle. The power of such analysis techniques is further discussed by Qualls and Boykins [28] and provides a basic tool for design analysis and optimization.

The environments of concern are the LEO environment of ISS and the deep space environment. They differ on account of the geomagnetic field. Although the GCR are part of the overall exposure, only the trapped radiations during quiet geomagnetic periods will be considered herein.

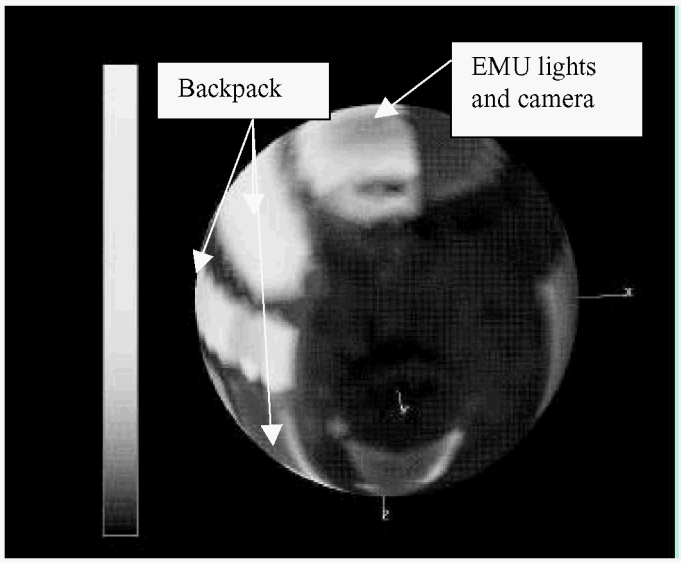

Figure 9-14. Visualization of the space suit shield materials distribution about a point in the sternum.

LEO OPERATIONS – The trapped environment near solar maximum is shown in **Figures 9-5** through **9-8** for this high inclination and relatively high altitude orbit. The attenuation of that environment is shown in **Figures 9-15** and **9-16** for low penetration depths. One can see from the figures that the doses can be quite high for low penetration depths and reduce quickly with increasing depth. The basal layer of the skin lies about 1 mm below the surface and the additional 0.28 g/cm^2 of fabric used in prior calculations would result in about 6 cGy per day from electrons neglecting self-shielding. The present estimate of the mean fabric penetration is 0.161 g/cm^2 with resultant exposures on the order of 14 cGy/day, or more than a factor of two higher than results for the prior model. The relative difference between the two fabric models will remain, although self-shielding will lower the total dose considerably. Although the protons likewise attenuate quickly at low penetration depths, the resultant exposure is not as large as that for electrons.

The dose incurred during a six-hour exposure for geomagnetic quiet times near solar maximum is not to be expected to a serious limiting factor. However, geomagnetic storms are observed during solar active years to increase the electron environment, over a period of approximately an hour or less, by three or four orders of magnitude greater than the quiet time levels shown in **Figures 9-5** and **9-15**. Even a modest amount of time in such an environment can lead to serious exposures, especially to the skin. The thresholds for the early radiation responses (deterministic effects as opposed to the stochastic effects such as cancer induction) are very narrow and a factor of two in exposure is extremely important to radiation health outcome [18,29].

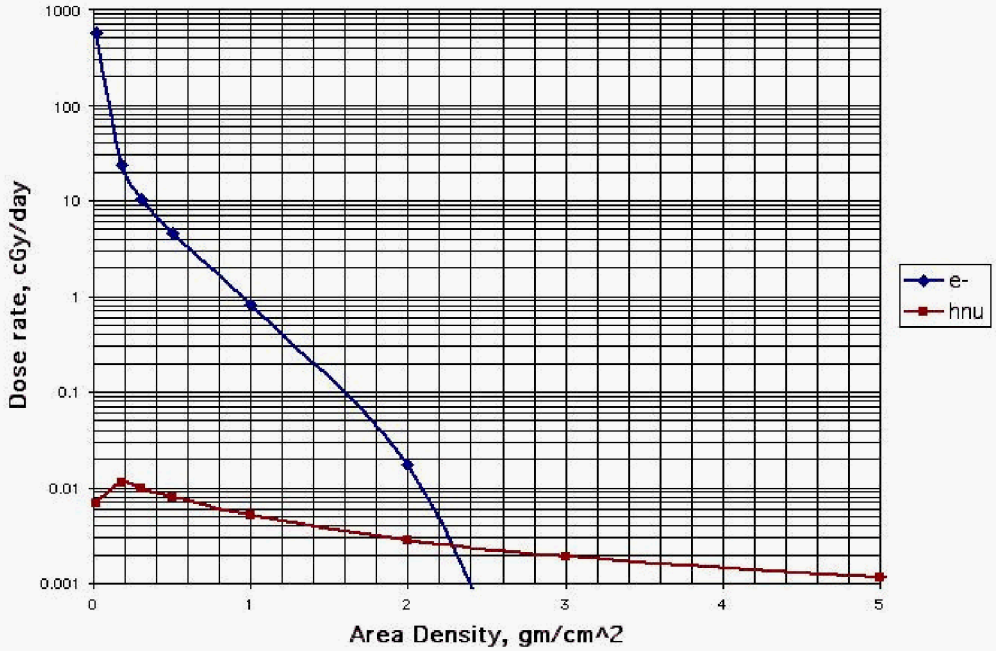

Figure 9-15. STS-48 electron and photon (h?) dose as a function of fabric thickness.

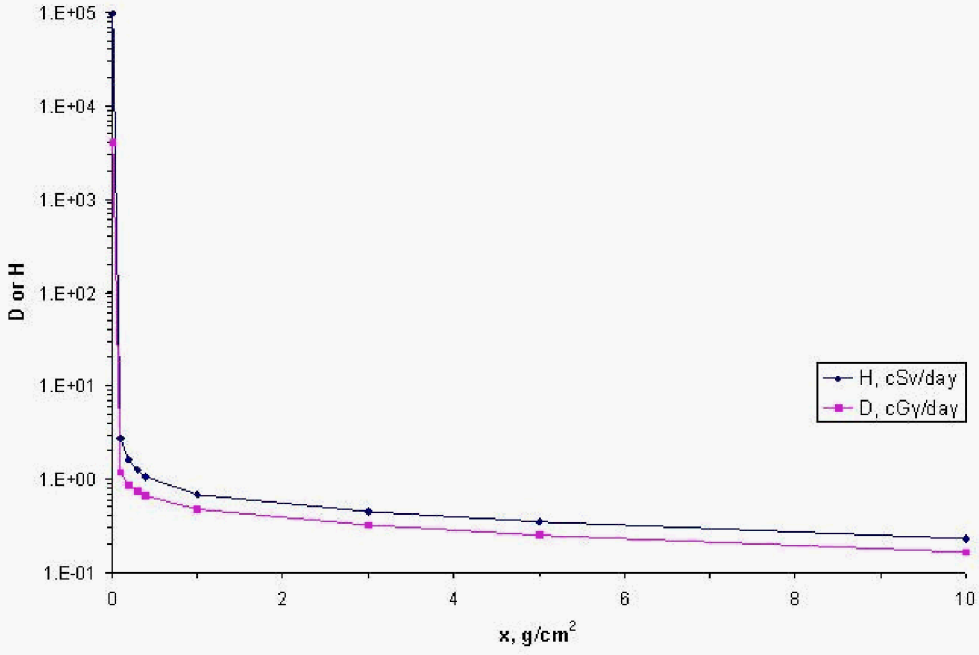

Figure 9-16. STS-48 proton daily dose and dose equivalent as a function of fabric thickness.

DEEP SPACE OPERATIONS – There are two issues in deep space exposures: the rates of cancer induction from GCRs and concern for a SPE. SPEs are of potentially grave concern in space exploration where astronauts will spend periods in poorly protected regions as the space suit. The August 4, 1972, SPE is the worst-case event for which some details of the low-energy proton spectrum was measured and used to analyze their importance to

astronaut health [18]. The single largest ground-level event observed is the February 23, 1956, event but little is known of the low-energy spectrum. The second largest ground-level event observed is that of September 29, 1989, and good details on the spectral properties [19] are available as shown in **Figures 9-9** and **9-10**. The importance of the September 29, 1989, event, which we evaluate herein, is that ten times the September 29, 1989, event is a proxy for the February 23, 1956, event.

The dose and dose equivalent in tissue from various components within a spherical shell of space suit fabric material is shown in **Figures 9-17** and **9-18**, with the totals in **Figure 9-19**. The dose is dominated by the proton fluence over most shielding thicknesses. The dose equivalent from helium ions gives an important contribution for thicknesses on the order of the space suit fabric. The heavier ions are always unimportant to the exposure.

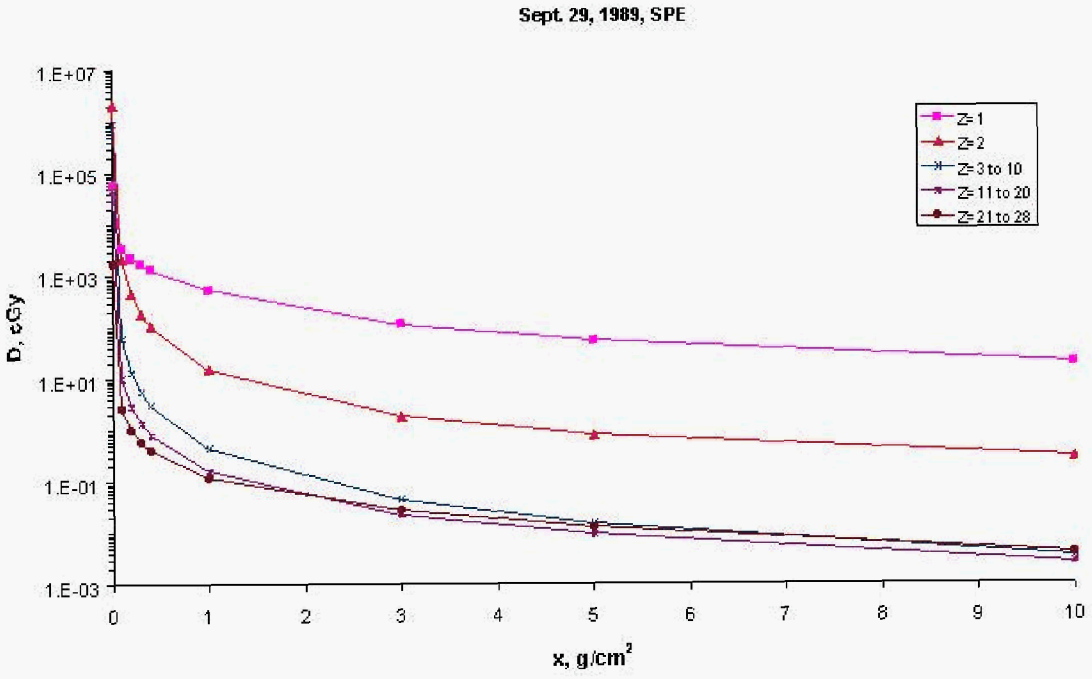

Figure 9-17. Dose within a fabric shield during the September 29, 1989, SPE.

It is clear from the results in **Figure 9-19** that very high skin exposures can be expected for this event. However, even modest amounts of additional shielding in the thermal micrometeoroid garment are expected to have important effects in reducing the exposures. Still, some caution in redesign is warranted since mobility and comfort to the astronaut is a key issue in space operations.

There is a slow but significant decline in dose and dose equivalent with larger shield thickness, indicating some advantage is to be gained by the more massive components of the suit and the self-shielding of critical tissues of the astronaut's body. These will be evaluated in terms of the CAM/CAF geometry and the present space suit model.

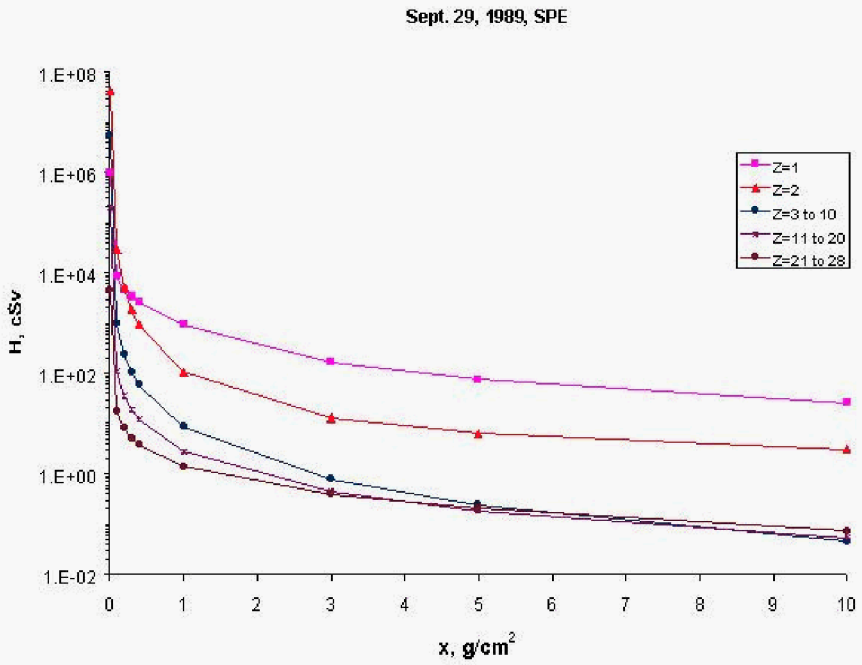

Figure 9-18. Dose equivalent within a fabric shield during the September 29, 1989, SPE.

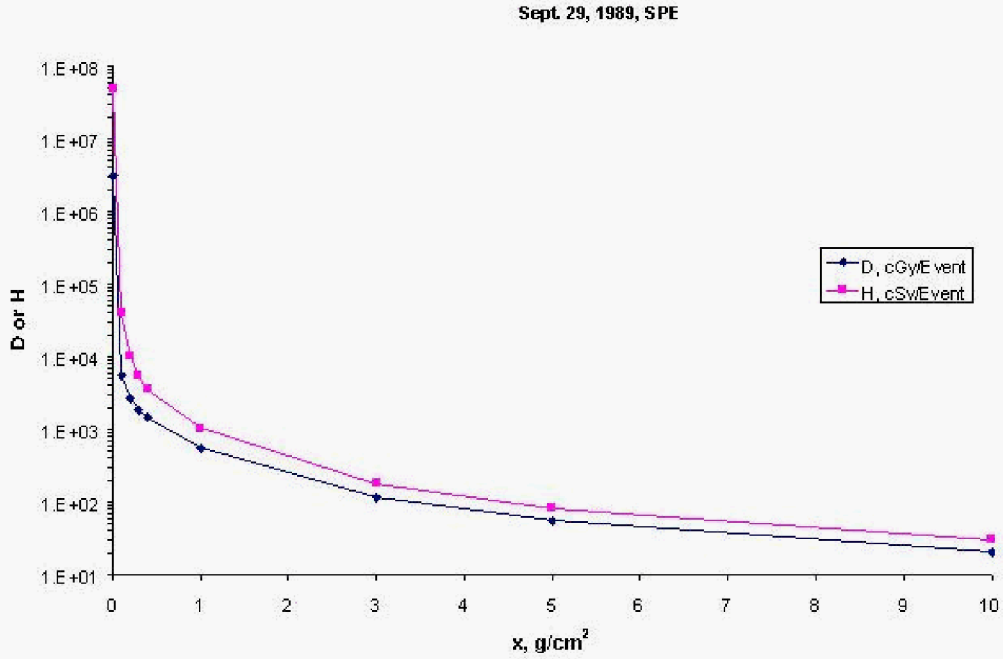

Figure 9-19. Total dose and dose equivalent within a fabric shield during the September 29, 1989, SPE.

9.8 CONCLUSION

It is clear from the present analysis and results that the space suit has some important features that will have some benefit for reducing the astronaut health risks under the extreme exposure conditions in space. Even so, some

weaknesses in the space suit design are already clear. Mainly, attention has presently been given to the space suit fabric (thermal micrometeoroid garment/LCVC) that is less effective in protecting the skin from exposure than previously assumed and could be greatly improved. It is clear that only modest additions to the fabric elements will have a large payoff in protection. What still needs addressed is the remaining more massive elements within the space suit and their effects on specific organ tissue exposures. This will be more fully addressed in the near future.

9.9 REFERENCES

1. Nealy, J.E. et al. Adv. Space Res. 17(2): 117-120, 1996.
2. Kozloski L.D., US Space Gear: Outfitting the Astronaut, Smithsonian Institution Press, Washington DC, 1994.
3. Severin G.I., Acta Astronautica 32(1): 15-23, 1994.
4. Abramov I.P., Acta Astronautica 36(1): 1-12, 1995.
5. Kosmo J.J., Nachtwey D.S., Hardy A. JSC/CTSD-SS-241, 1-24-1989.
6. Ross A.J. et al. NASA CP 3360, 1997.
7. Wilson, J.W. SAE 01ICES-299, 2001.
8. Wilson, J.W. Health Phys. 28:812-813, 1975.
9. Wilson, J.W. et al. NASA TP-3668, 1997.
10. Kase, Paul G., "Computerized Anatomical Model Man, " Report AFWL-TR-69-161, Air Force Weapons Laboratory, Kirtland Air Force Base, NM, January 1970.
11. Billings, M.P., and W.R. Yucker, "Summary Final Report. The Computerized Anatomical Man (CAM) Model," Report MDC G4655, McDonnell Douglas Astronautics Company, Huntington Beach, CA, September 1973.
12. Jordan, T.M., "QUAD, A Computer Subroutine for Ray Tracing in Quadric Surface Geometries," Douglas Report SM-46333, 1964.
13. Yucker, W.R., and S.L. Huston, "Computerized Anatomical Female. Final Report," Report MDC H 6107, McDonnell Douglas Corporation, Huntington Beach, CA, September 1990.
14. Yucker, W.R., "Computerized Anatomical Female Body Self-Shielding Distributions," Report MDC 92H0749, McDonnell Douglas Corporation, Huntington Beach, CA, March 1992.
15. Atwell, W., "Anatomical Models for Space Radiation Applications: An Overview;" Invited paper (F2.4-M.1.06) presented at the Committee on Space Research (COSPAR), Washington, DC, August 28 - September 5, 1992.
16. Atwell, W., A. C. Hardy, and L. Peterson, "Organ Radiation Doses and Lifetime Risk of Excess Cancer for Several Space Shuttle Missions," Invited paper # F2.4-001, Committee on Space Research (COSPAR), Hamburg, Germany, July 11-21, 1994.
17. Wilson, J.W. et al. NASA/TP-1999-209369, 1999.

18. Wilson, J.W. et al. Radiat. Measurement 30: 361-382; 1999.

19. Kim, H.-Y. M. et al. NASA TP/1999-209320, 1999.

20. Wilson, J. W. et al., *Transport Methods and Interactions for Space Radiations.* NASA Reference Publication, RP-1257, 1991.

21. Clowdsley, M. S. et al., Cana. J. Phys. 78: 45-56, 2000.

22. Tabata, T., et al., Nucl. Inst. & Meth. 103: 85-91, 1972.

23. Kobetich, E. J. and Katz, R., Nucl. Inst. & Meth. 71: 226-230, 1969.

24. Kobetich, E. J. and Katz, R., Phys. Rev. 170(2): 391-396, 1968.

25. Cucinotta, F.A.; Katz, R.; and Wilson, J.W.: Radial Distributions of Electron Spectra From High-Energy Ions. Radiat. Environ. Biophysics 37, 259-265, 1998

26. Seltzer, S. M. and Berger, M. J., Nucl. Inst. & Meth. B12: 95, 1985.

27. Halbleib, J. A. and Morel, J. E., Nucl. Sci. Eng., 70: 219, 1979.

28. Qualls, G.D. and Boykins, R., Space Radiation Shielding Analysis by CAD Techniques. NASA CP 3360, pp. 365-382; 1997.

29. NCRP, Guidance on Radiation Received in Space Activity, NCRP Report No. 98, 1989.

CONTACT

b.m.anderson@larc.nasa.gov